EPJ Web of Conferences **3**, 03015 (2010)
DOI:10.1051/epjconf/20100303015

$\bar{K}N$ dynamics at and near threshold energies

A. Cieplý[1,a] and J. Smejkal[2]

[1] Nuclear Physics Institute, 250 68 Řež, Czech Republic
[2] Institute of Experimental and Applied Physics, Czech Technical University in Prague, Horská 3a/22, 128 00 Praha 2, Czech Republic

Abstract. We have constructed effective separable meson-baryon potentials to match the equivalent chiral amplitudes up to the second order in external meson momenta. The parameters of the model were fitted to the threshold and low energy K^-p data including the 1s level characteristics of the kaonic hydrogen atom. We discuss the results of our fits and use the model to calculate the $\pi\Sigma$ mass spectrum and the energy dependence of the K^-N amplitudes.

1 Introduction

The meson-baryon interactions at low energies have become a testing ground for theoretical models based on chiral symmetry. In the SU(2) sector the chiral perturbation theory (ChPT) proved to be quite successful thanks to very small current masses of the u and d quarks. The smallness of the pion mass also complies well with its presumed origin as that of the Goldstone boson. The situation becomes more intriguing once we enter the strange sector. Especially, the treatment of the kaon-nucleon interaction at low energies requires a special care. Unlike the pion-nucleon interaction the $\bar{K}N$ dynamics is strongly influenced by the existence of the $\Lambda(1405)$ resonance, just below the K^-p threshold. This means that the standard chiral perturbation series do not converge. Fortunately, one can use non-perturbative coupled channel techniques to deal with the problem and generate the $\Lambda(1405)$ resonance dynamically. Though such approach violates the crossing symmetry it has proven quite useful and several authors have already applied it to various low energy meson-baryon processes [1]-[6].

Currently, the most popular approach to low energy $\bar{K}N$ interactions is based on dispersion relation for the inverse of the T-matrix and on the dimensional regularization of the scalar loop integral [7]. The N/D scheme may be so attractive because it uses the language of high energy physics and employs the quantum field techniques. The drawback of the method is that the coupled channel calculations are performed almost exclusively on-shell which makes the model less suitable for a treatment of many body systems, in particular for the Faddeev type calculations (e.g. of the $\bar{K}NN$–$\pi\Sigma N$ system [8]).

We have opted for a more traditional approach based on the coupled channel Lippman-Schwinger equations. The meson-baryon potentials that enter the LS equations are related to the underlying chiral Lagrangian and incorporate naturally the off shell effects due to the adopted separable form. The model was developed in Ref. [1] and we applied it to the fits of all available K^-p data [9], [10].

We devoted our analysis to simultaneous description of the kaonic hydrogen characteristics, the K^-p threshold branching ratios and the low energy K^-p cross sections. The repulsive character of the K^-p strong interaction at threshold was first confirmed at KEK by the measurement of the 1s energy level shift and absorption width in kaonic hydrogen atom [11]. More recently, the precision of the experimental data was significantly improved by the DEAR collaboration in Frascati [12]. Unfortunately, the DEAR results seem at odds [4], [5] with the K^-p scattering length extrapolated from the scattering measurements [13]. Thus, we decided to check whether the parameters of our model can be tuned in fits to the relevant K^-p data including the DEAR results. A more detailed account of our work was given in Refs. [9] and [10] and here we concentrate only on the main results.

2 Separable potentials

The necessary ingredient needed to calculate the impact of strong interaction on K-atomic energy levels is the kaon-nuclear optical potential. In the case of kaonic hydrogen and multiple channels it means the potential matrix. We follow the approach of Ref. [1] and construct the strong interaction part of the potential matrix as effective transition amplitudes that give the same (up to the order $O(q^2)$ of the external meson momenta) s-wave scattering lengths as are those derived from the underlying chiral Lagrangian. While the authors of Ref. [1] restricted themselves only to the first six meson-baryon channels that are open at the $\bar{K}N$ threshold we employ all ten coupled meson-baryon channels: $\pi^0\Lambda$, $\pi^0\Sigma^0$, $\pi^-\Sigma^+$, $\pi^+\Sigma^-$, K^-p, $\bar{K}^0n$, $\eta\Lambda$, $\eta\Sigma^0$, $K^0\Xi^0$, and $K^+\Xi^-$ (ordered according to their threshold energies).

[a] e-mail: cieply@ujf.cas.cz

The strong interaction potential matrix is given in the separable form

$$V_{ij}(k,k') = \sqrt{\frac{1}{2E_i}\frac{M_i}{\omega_i}}\, g_i(k)\, \frac{C_{ij}}{f^2}\, g_j(k') \sqrt{\frac{1}{2E_j}\frac{M_j}{\omega_j}} \quad , \quad (1)$$

in which the momenta k and k' refer to the meson-baryon c.m. system in the i and j channels, respectively. The kinematical factors $\sqrt{M_j/(2E_j\omega_j)}$ guarantee a proper relativistic flux normalization with the meson energy E_j and the baryon mass and energy M_j and ω_j, all taken in the c.m. system of channel j. The off shell form factors,

$$g_j(k) = \frac{1}{1+(k/\alpha_j)^2} \quad , \quad (2)$$

introduce the inverse range radii α_j that characterize the radius of interactions in various channels. Finally, the parameter $f \simeq 100$ MeV (a value between the empirical pion and kaon decay constants) stands for the pseudoscalar meson decay constant in the chiral limit and the coupling matrix C_{ij} is determined by chiral SU(3) symmetry and includes terms up to the second order in the meson c.m. kinetic energies.

When the effective meson-baryon potentials (1) are constructed to match the Born amplitudes generated by the chiral Lagrangian the low energy constants (the couplings at various terms in the Lagrangian) combine to the couplings C_{ij} that bind the considered meson-baryon states. Thus, the chiral symmetry of meson-baryon interactions is reflected in the structure of the C_{ij} coefficients derived directly from the Lagrangian. The general structure of the couplings reads as

$$\begin{aligned} C_{ij} = C_{ij}^{(\mathrm{WT})}\, \frac{E_i' + E_j'}{4} \; + \; C_{ij}^{(s)}\, \frac{E_i E_j}{2M_0} + \quad (3) \\ + \; C_{ij}^{(u)}\, \frac{1}{3M_0} \left(2m_i^2 + 2m_j^2 + \frac{m_i^2 m_j^2}{E_i E_j} - \tfrac{7}{2} E_i E_j \right) + \\ + \; C_{ij}^{(mm)} \left(m_i^2 + m_j^2 \right) \; + \; C_{ij}^{(\chi \mathrm{b})} \left(m_K^2 - m_\pi^2 \right) + \; C_{ij}^{(EE)}\, E_i E_j \; , \end{aligned}$$

where the primed meson energies E_j' include the relativistic correction, $E_j' = E_j + (E_j^2 - m_j^2)/(2M_0)$, with m_j denoting the meson mass in the channel j and M_0 standing for the baryon mass in the chiral limit. The actual composition of the coefficients $C_{ij}^{(.)}$ was given it Ref. [10]. Here we only mention that the terms marked by the superscripts "WT", "s" and "u" correspond to the leading Weinberg-Tomozawa contact interaction and to the direct and crossed Born amplitudes, respectively. The remaining parts contribute to the contact interaction in the next-to-leading (*i.e.* q^2) order.

The potential of Eq. (1) is used in the standard coupled channel Lippman-Schwinger equations to compute the low energy $\bar{K}N$ cross sections and branching ratios from the resulting transition amplitudes. At the same time the potential is also used to solve the K^--proton bound state problem. This way the characteristics of the 1s level in kaonic hydrogen are obtained by direct calculation, not by relating them to the K^-p scattering length by means of the Deser-Trueman formula [14] or its improved version [15]. We feel that a direct calculation of the kaonic hydrogen characteristics is becoming necessary in view of the expected precision of the current K-atomic SIDDHARTA experiments on hydrogen and deuterium [16].

3 Results

3.1 $\bar{K}N$ data fit

The three precisely measured threshold branching ratios [13] are

$$\begin{aligned} \gamma &= \frac{\sigma(K^-p \to \pi^+\Sigma^-)}{\sigma(K^-p \to \pi^-\Sigma^+)} = 2.36 \pm 0.04 \; , \quad (4) \\ R_c &= \frac{\sigma(K^-p \to \text{charged particles})}{\sigma(K^-p \to \text{all})} = 0.664 \pm 0.011 \; , \\ R_n &= \frac{\sigma(K^-p \to \pi^0\Lambda)}{\sigma(K^-p \to \text{all neutral states})} = 0.189 \pm 0.015 \; . \end{aligned}$$

They impose quite tight constraints on any model applied to the $\bar{K}N$ interactions at low energies.

The cross sections of K^-p initiated reactions are not determined so accurately, thus they do not restrict the fits so much. We consider only the experimental data taken at the kaon laboratory momenta $p_{LAB} = 110$ MeV (for the K^-p, $\bar{K}^0n$, $\pi^+\Sigma^-$, $\pi^-\Sigma^+$ final states) and at $p_{LAB} = 200$ MeV (for the same four channels plus $\pi^0\Lambda$ and $\pi^0\Sigma^0$). Although some authors include in their fits the experimental cross sections at all available kaon momenta we feel that such approach unduely magnifies the importance of this particular set of data at expense of all other measurements that are not represented by so many data points. Anyway, our results show that the inclusion of the cross section data taken at many kaon momenta is not necessary since the fit at just 1–2 points fixes the cross section magnitude and the energy dependence is reproduced nicely by the model.

We apply the same philosophy to the measured $\pi\Sigma$ mass distribution and fit only the position of the peak at 1395 MeV instead of fitting the complete measured spectra. In a manner of Ref. [7] we also assume that the $\pi\Sigma$ mass distribution originates from a generic s-wave isoscalar source which couples to the $\bar{K}N$ and $\pi\Sigma$ $I = 0$ states. Since the measured event distribution is not normalized, only the ratio of the relevant couplings $r = r_{\bar{K}N}/r_{\pi\Sigma}$ is of significance. In other words, we assume that the observed $\pi\Sigma$ spectrum complies with the prescription

$$dN_{\pi\Sigma}/dE \sim \left| T_{\pi\Sigma,\pi\Sigma}(I=0) + r_{KN/\pi\Sigma}\, T_{\pi\Sigma,\bar{K}N}(I=0) \right|^2 p_{\pi\Sigma} \quad (5)$$

where the ratio $r_{KN/\pi\Sigma}$ is energy independent. In general, the ratio should be a complex number but (to further simplify the matter) we consider only real values in our fits. Though the reality may not be so simple the ansatz looks

appropriate for simulating the dynamics of the $\Lambda(1405)$ resonance.

Finally, we include the DEAR results [12] on the strong interaction shift ΔE_N and the decay width Γ of the 1s level in kaonic hydrogen:

$$\Delta E_N(1s) = (193 \pm 43)\ \text{eV}, \quad \Gamma(1s) = (249 \pm 150)\ \text{eV}\ . \quad (6)$$

Thus, we end up with a total of 16 data points in our fits.

The parameters of our model are:
a) the couplings of the chiral Lagrangian which enter the coefficients C_{ij} (concerning the specification of our chiral Lagrangian and its various chiral couplings we refer the reader to Refs. [1] and [10])
b) the inverse range radii α_j that determine the off-shell form factors $g_j(k)$, Eq. (2)
c) the ratio $r_{KN/\pi\Sigma}$ specifying the relative coupling of the $\bar{K}N$ and $\pi\Sigma$ channels to the $\Lambda(1405)$ resonance.

Before performing the fits we reduce the number of the fitted parameters in the following way. First, the axial couplings D and F have already been established in the analysis of semileptonic hyperon decays, $D = 0.80$, $F = 0.46$ ($g_A = F + D = 1.26$) [17]. Then, we fix the couplings b_D and b_F to satisfy the approximate Gell-Mann formulas for the baryon mass splittings, $b_D = 0.064\ \text{GeV}^{-1}$ and $b_F = -0.209\ \text{GeV}^{-1}$. Similarly, we determine the coupling b_0 and the baryon chiral mass M_0 from the relations for the pion-nucleon sigma term $\sigma_{\pi N}$ and for the proton mass (see [10]). Since the value of the pion-nucleon σ-term is not well established we enforce four different options, $\sigma_{\pi N}$ = (20–50) MeV, which cover the interval of the values considered by various authors. We also use the Cayley-Hamilton identity to reduce the number of the second order d-couplings and set $d_2 = 0$. It means that the only low energy constants (Lagrangian couplings) that remain to be fitted are the pseudoscalar meson decay constant f and four d-couplings, d_D, d_F, d_0, and d_1. Finally, we reduce the number of the inverse ranges α_i to only five: α_{KN}, $\alpha_{\pi\Lambda}$, $\alpha_{\pi\Sigma}$, $\alpha_{\eta\Lambda/\Sigma}$, $\alpha_{K\Xi}$. Thus we are left with 11 free parameters: the five inverse ranges, the pseudoscalar meson-baryon chiral coupling f, the ratio $r_{KN/\pi\Sigma}$ of Eq. (5) and four d-couplings.

The Table 1 shows the results of our χ^2 fits compared with the relevant experimental data. The resulting χ^2 per data point indicate satisfactory fits. It is worth noting that their quality and the computed values do not depend much on the chosen value of the $\sigma_{\pi N}$ term.

The strong interaction energy shift of the 1s level in kaonic hydrogen is reproduced well but we were not able to get a satisfactory fit of the 1s level energy width as our results are significantly larger than the experimental value. This result is in line with the conclusions reached by Borasoy, Meissner and Nissler [5] on the basis of their comprehensive analysis of the K^-p scattering length from scattering experiments. However, when considering the interval of three standard deviations and also the older KEK results [11] (which give less precise but larger width) we cannot conclude that kaonic hydrogen measurements contradict the other low energy $\bar{K}N$ data. We hope the new SIDDHARTA experiment [16] performed in Frascati will clarify the situation concerning the kaonic hydrogen characteristics. In view of its expected precision it becomes necessary to solve the K^-p bound state problem exactly (as we do here) rather than relate the K-atomic characteristics to the K^-p scattering length. We have shown [9] that the difference may be as large as about 10%, which is more than the anticipated precision of the SIDDHARTA measurement.

Table 1. The fitted $\bar{K}N$ threshold data

$\sigma_{\pi N}$ [MeV]	χ^2/N	ΔE_N [eV]	Γ [eV]
20	1.33	214	718
30	1.29	260	692
40	1.35	195	763
50	1.37	289	664
exp	-	193(43)	249(150)

$\sigma_{\pi N}$ [MeV]	γ	R_c	R_n
20	2.368	0.653	0.189
30	2.366	0.655	0.188
40	2.370	0.654	0.191
50	2.366	0.658	0.192
exp	2.36(4)	0.664(11)	0.189(15)

In Figure 1 we present the low energy K^-p initiated cross sections. The results obtained for various adopted values of $\sigma_{\pi N}$ are practically undistinguishable with the only exception at low kaon momenta in the elastic channel. This observation is rather puzzling since the experimental cross sections are not so much restrictive as the threshold branching ratios. Apparently, the parameter space is flexible enough to accommodate the fitted values. Though we declined from using all experimental data in our fits and took only the data points available for the selected kaon laboratory momenta $p_{LAB} = 110$ MeV and $p_{LAB} = 200$ MeV, the description of the data is quite good. Specifically, we do not observe the lowering of the calculated cross sections in the elastic K^-p channel reported by Borasoy et al. [4] for their fits including the DEAR kaonic hydrogen characteristics. Though our K^-p cross sections are also slightly below the experimental data the difference is not significant. In addition, the inclusion of electromagnetic corrections discussed in Ref. [4] should partly improve the description for the lowest kaon momenta.

3.2 $\Lambda(1405)$ resonance

The origin and structure of the $\Lambda(1405)$ resonance observed in the $\pi\Sigma$ mass spectrum are an actively pursued topic. The coupled channel meson-baryon models based on chiral symmetry generate the resonance dynamically and it appears that there are two poles in the complex energy plane that may contribute to the observed spectrum [7]. This recent discovery has stimulated both the theoretical debates as well as experimental efforts aiming at a better understanding of the $\Lambda(1405)$ structure.

The Fig. 2 visualizes the $\pi\Sigma$ mass distribution computed for the parameter sets related to $\sigma_{\pi N} = 40$ MeV.

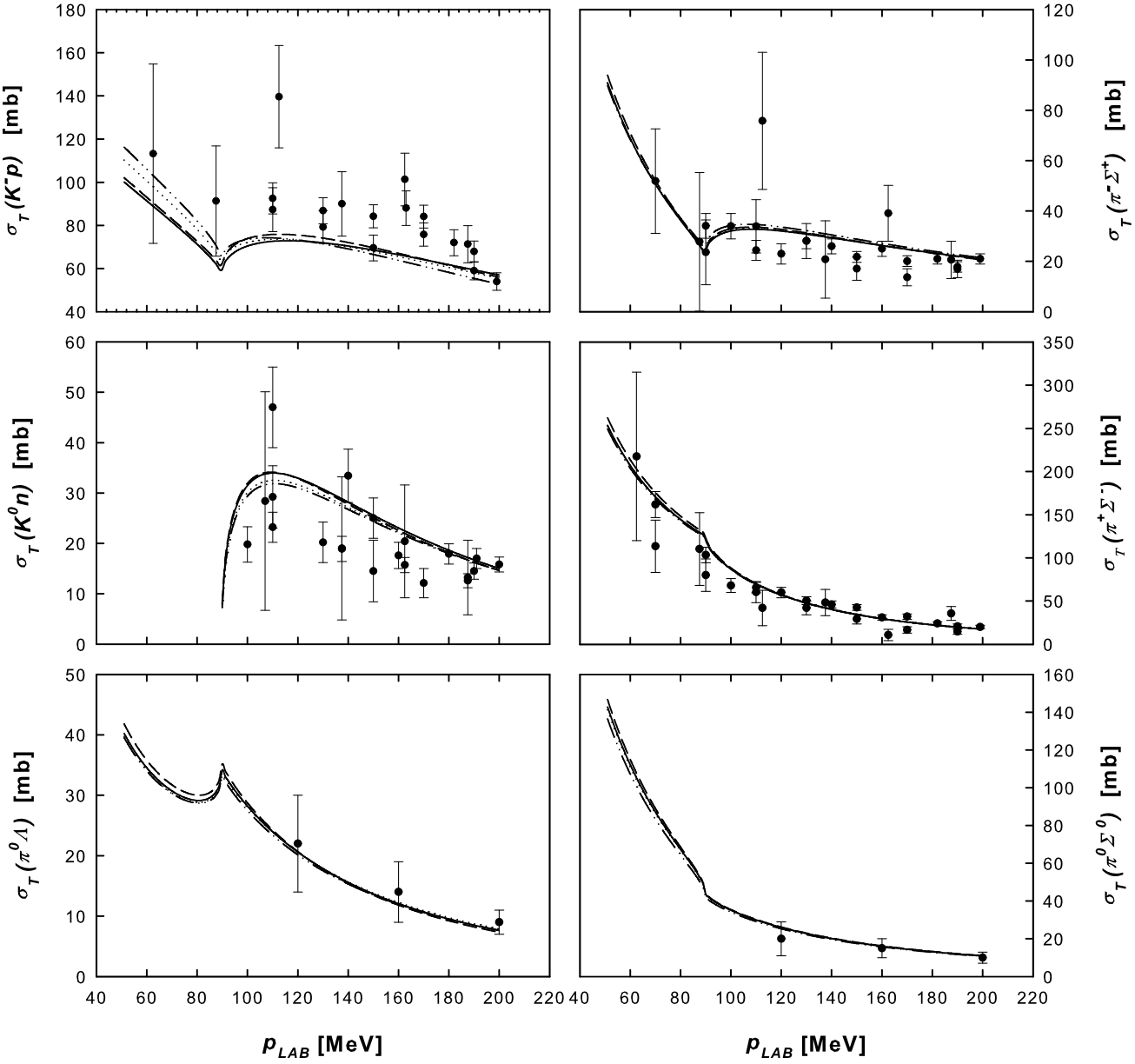

Fig. 1. Total cross sections for K^-p scattering and reactions to the meson-baryon channels open at low kaon laboratory momenta p_{LAB}. The experimental data are the same as those compiled in Fig. 1 of Ref. [1]. Our results obtained for $\sigma_{\pi N}$ = 20, 30, 40 and 50 MeV are visualized by the full, dotted, dashed and dot-dashed lines, respectively.

In addition to the distribution obtained for the present fit (and represented by a full line in the figure) we also show (dashed line in the figure) the $\pi\Sigma$ spectrum generated for the pertinent parameter set of Ref. [9] and $r_{KN/\pi\Sigma} = 1$. It peaks at 1391 MeV and we would need $r_{KN/\pi\Sigma} = 2.6$ to shift the spectrum to peak at 1395 MeV. The shape of the spectrum is not much affected by tuning the parameter $r_{KN/\pi\Sigma}$ within reasonable limits. Just for a reference we also show the spectra obtained by assuming that the $I = 0$ resonance originates only from the $\pi\Sigma$ channels ($r_{KN/\pi\Sigma} = 0$, dotted line in Fig. 2) or that it is formed exclusively from the $\bar{K}N$ channels ($1/r_{KN/\pi\Sigma} = 0$, dot-dashed line). These two lines represent a kind of boundaries on the shape and peak position of the spectra in a situation when the low energy constants are fixed at the values obtained in our current fit for $\sigma_{\pi N} = 40$ MeV. Similar picture can also be drawn for the other choices of $\sigma_{\pi N}$.

The experimental data shown in Fig. 2 come from three different measurements [18], [19], [20], all exhibiting a prominent structure around 1400 MeV. As the observed spectra are not normalized we have rescaled the original data as well as our computed distributions to give 1000 events in the chosen energy interval (from 1330 to 1440 MeV). The three measurements give $\pi\Sigma$ distributions that look mutually compatible. We have not included in the figure the $K^-p \to \Sigma^0\pi^0\pi^0$ data measured by the Crystal Ball

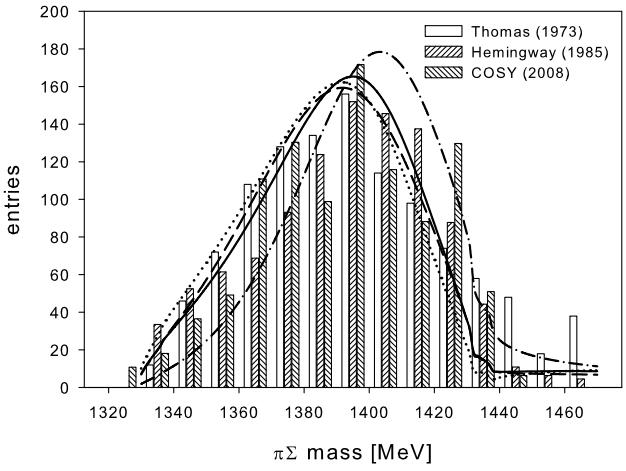

Fig. 2. The $\pi\Sigma$ mass distribution. Our results are compared with the experimental data taken from Refs. [18], [19] and [20]. The full line was obtained for the parameter set of the present work, the dashed line for the one of Ref. [9], both related to $\sigma_{\pi N} = 40$ MeV. See the text for explanation on the dotted and dash-dotted lines.

Collaboration [21] as they yield a slightly different distribution with a peak structure around 1420 MeV. The two identical pions in the final state of the later reaction complicate a comparison with the other experiments, so we find it questionable to relate our computed lineshape to the one observed in [21] without employing fully the dynamics of the particular reaction as it was done in [22].

The values of $r_{KN/\pi\Sigma}$ obtained in our fits (and presented in the Table 2) are compatible with similar findings by other authors [23], [4]. Since the magnitude of $r_{KN/\pi\Sigma}$ is of the order of one it looks that both the $\bar{K}N$ and the $\pi\Sigma$ states contribute to the $I = 0$ resonance identified with $\Lambda(1405)$ with a comparable strength. In other words, the inclusion of the initial $\bar{K}N$ channels in the model driven by Eq. (5) is important. This is fully in line with the well known fact that the $\Lambda(1405)$ resonance does couple strongly to the K^-p state. Unfortunately, the experimental data are not precise enough to distinguish between various values of $r_{KN/\pi\Sigma}$ which is demonstrated in Fig. 2 by comparing our best fit results with those generated for the boundary values of $r_{KN/\pi\Sigma}$. Since a good description of the spectrum can already be achieved without its inclusion in the fits one may argue that the dynamics of the chiral model is fixed by the threshold (and low energy) observables of K^-p interactions. However, the data clearly prefer a positive sign of $r_{KN/\pi\Sigma}$, *i.e.* a constructive interference of the contributions provided by the $\pi\Sigma$ and $\bar{K}N$ channels to the resonance. For the negative values of $r_{KN/\pi\Sigma}$ the peak moves to energies lower than the one obtained at the $r_{KN/\pi\Sigma} = 0$ boundary and the computed spectrum no longer matches the experimental one.

The interest in the $\pi\Sigma$ mass distribution has arisen since discovering that the chiral meson-baryon dynamics generates two poles in the complex energy plane that can be related to the $\Lambda(1405)$ resonance. In the Table 2 we show the

Table 2. The complex energies of the poles relevant to the $I = 0$ resonance.

$\sigma_{\pi N}$ [MeV]	$r_{KN/\pi\Sigma}$	Re z_1 [MeV]	Im z_1 [MeV]	Re z_2 [MeV]	Im z_2 [MeV]
20	1.28	1395	−49	1456	−77
30	1.32	1398	−51	1441	−76
40	0.37	1401	−41	1519	−112
50	0.54	1406	−39	1436	−138

positions of the poles generated by our model. They appear on the unphysical Riemann sheet accessed when crossing the real axis between the thresholds of the $\pi\Sigma$ and the $\bar{K}N$ channels. The position of the lower (with the lower value of the real part of the complex energy) pole is more or less stable and does not depend much on the choice of the parameter set. Its complex energy $z \approx (1400 - \mathrm{i}\,45)$ MeV can clearly be associated with the observed $\pi\Sigma$ mass spectrum. On the other hand, the higher (in terms of Re z) pole is located further from the real axis and its position vary with the chosen parameter set. We have also noted that parameter sets obtained for various local χ^2 minima lead to different positions of this pole even if they correspond to the same choice of the πN sigma term.

Interestingly, neither of the two poles is located so close to the real energy axis as other authors claim. This feature can be explained by a different parametrization of our model. It was already shown by Borasoy et al. [4] that the second pole moves away from the real axis when the second order terms are included in the chiral Lagrangian. Our observations confirm this. When we performed a fit (for $\sigma_{\pi N} = 40$ MeV) with the next-to-leading order terms neglected we located the poles at $z_1 = (1368 - \mathrm{i}\,42)$ MeV and $z_2 = (1441 - \mathrm{i}\,22)$ MeV. Although the second pole remains above the $\bar{K}N$ threshold while other authors observe it about 10 MeV below the threshold, the closeness of the pole to the real axis seems to be related to the omission of the next-to-leading order corrections in the chiral Lagrangian. We also noted that our fits with interaction restricted only to the Weinberg-Tomozawa term require very large values of the parameter $r_{KN/\pi\Sigma}$, typically $r_{KN/\pi\Sigma} \gtrsim 10$. This means that in such a case the resonance observed in the $\pi\Sigma$ mass spectrum couples much stronger to the $\bar{K}N$ channels than to the $\pi\Sigma$ ones.

Though the quality of the fit is much worse without the second order terms (we got $\chi^2/N = 3.1$ in the case mentioned here), most of the K^-p data are still reproduced quite well. On the other hand Hyodo and Weise [24], who locate the $\bar{K}N$ quasibound state at $\sqrt{s} \simeq 1420$ MeV, use a parametrization that is not suitable for a description of all relevant $\bar{K}N$ data, specifically they do not reproduce (as one can check in [25]) the precise threshold rates, Eq. (4). Borasoy et al. [4] do fit all relevant K^-p data including the threshold rates, however their pole at 1420 MeV moves away from the real axis (and to lower energies) when they include the DEAR data in their fits. When they compromise the DEAR data with those from K^-p reactions they get the pole quite close to where we see it. Therefore, it

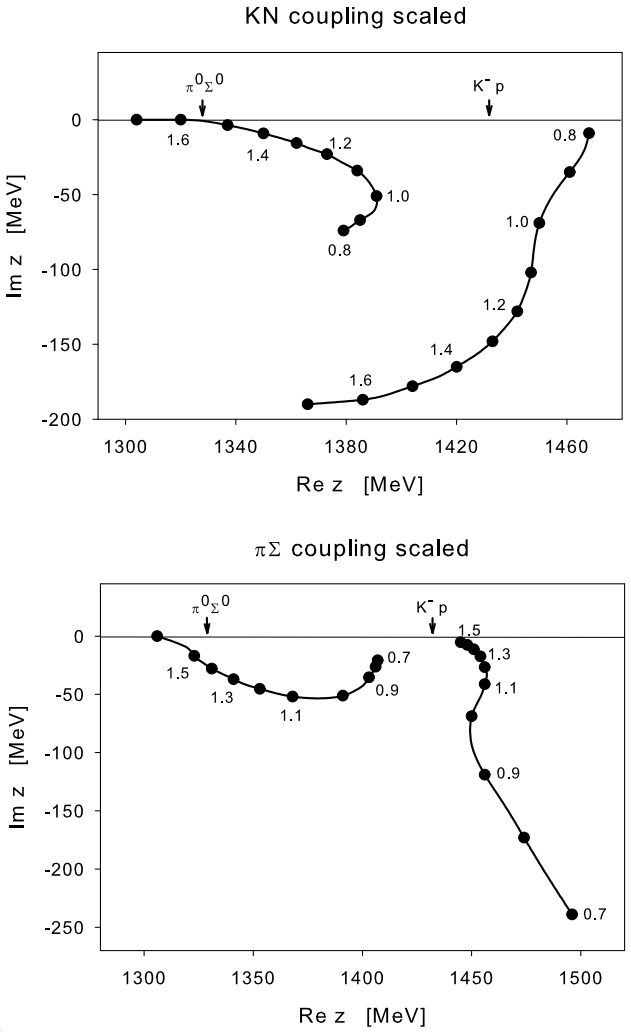

Fig. 3. Trajectories of the poles related to $\Lambda(1405)$ upon scaling the couplings in the $\bar{K}N$ (top panel) and $\pi\Sigma$ (bottom panel) channels. The $\pi^0\Sigma^0$ and K^-p thresholds are marked by arrows.

looks plausible that the remaining differences in exact localization of the poles can be attributed either to model specifics or to the fact that the models do not reproduce all observed experimental data on the same footing.

In a comment made by one of us and A. Gal [26] we also showed that the position of the poles can change drastically when playing with the meson-baryon channel couplings. The pole movement in the complex energy plane is visualized in Figure 3 taken from Ref. [26]. Once again the trajectory of the lower pole indicates that it should be associated with the $\pi\Sigma$ mass spectrum since for sufficiently strong couplings the pole changes into a bound state located below the $\pi\Sigma$ threshold. The trajectory of the pole located above the K^-p threshold takes it away from the real axis and supports our observation that a position of this pole (and how far it is from the real axis) is much more model dependent.

The shape of the $\pi\Sigma$ mass spectrum is determined by the positions of the two $I = 0$ poles and by the relative couplings of the $\pi\Sigma$ and $\bar{K}N$ states to the poles (the parameter $r_{KN/\pi\Sigma}$ in our model). It is obvious that the observed spectrum does not resemble a typical Breit-Wigner resonance. While this can be attributed to an interplay of two resonances that are relatively close to the real axis [23] we can explain the $\pi\Sigma$ distribution without any resonance that sits in a vicinity of the real axis. In our model the observed structure is not of the Breit-Wigner type simply because there is no pole sufficiently close to the real axis. We hope that new results from experiments dedicated to exploration of the $\Lambda(1405)$ structure will be able to distinguish between those two pictures.

3.3 K^-N amplitudes

The K^-p amplitudes generated by our model are shown in Figure 4 for the c.m.s. energies from 1300 MeV to 1500 MeV. While all our fits (for the various choices of the $\sigma_{\pi N}$ term) provide practically the same K^-p amplitudes at and above the K^-p threshold the extrapolation of the amplitudes to energies below the threshold is not uniform. Specifically, the energy dependence of the K^-p amplitude obtained for $\sigma_{\pi N} = 50$ MeV deviates most from the other three curves. On the other hand, the two curves obtained for $\sigma_{\pi N} = 20$ MeV and 40 MeV are very close to each other.

Once the low-energy constants of the chiral Lagrangian and the inverse ranges of meson-baryon interactions are fixed to the K^-p data the model provides us with predictions for other interactions of the meson octet with the baryonic one. Here we present our results for the K^-n amplitude. The related coupled channels are represented by the following ones: $K^-\Lambda$, $\pi^-\Sigma^0$, $\pi^0\Sigma^-$, K^-n, $\eta\Sigma^-$, $K^0\Xi^-$ (listed in order of the respective thresholds).

In Figure 5 we show our results for the elastic K^-n amplitude as a function of the c.m.s. energy. It is a bit surprising to see that the calculated amplitudes depend on the choice of the parameter set (related to the value of the $\sigma_{\pi N}$ term) not only for energies below the K^-n threshold but above it too. At the K^-n threshold the variations in the real part of the elastic amplitude make as much as some 30%. Below the threshold the relative differences between the four curves are also larger than those we got for the K^-p amplitude. It is also worth noting that for energies below the threshold the real part of the K^-n amplitude follows a different trend than the one reported in Refs. [4] and [24]. Specifically, our Re f_{K^-n} is either a slightly decreasing or a more or less constant function of the energy while in [4] and [24] it turned out as monotonically increasing function of energy below the threshold. While the authors of the first paper [4] work with the physical meson and baryon masses and their approach is similar to ours (parameters fitted to K^-p data used to compute the K^-n amplitude) the results of the more recent work by Hyodo and Weise [24] were obtained in a model that adopts fully the isospin symmetry and does not aim at a realistic description of the K^-p threshold branching ratios. Since the other authors do not incorporate off-shell effects and use a different formulation of the $\bar{K}N$ dynamics it is difficult to trace the origin of the observed differences.

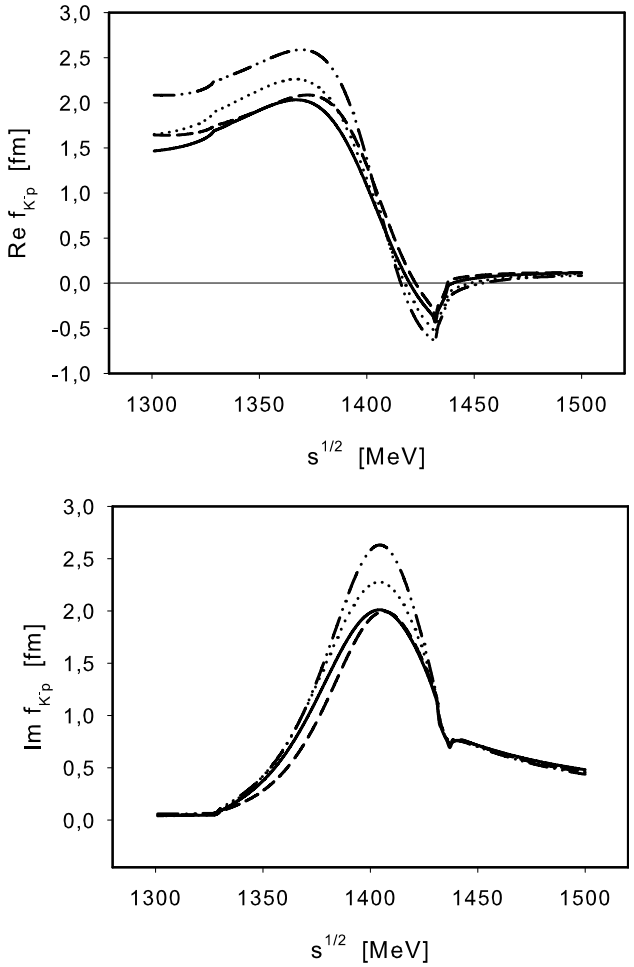

Fig. 4. The real (top panel) and imaginary (bottom panel) parts of the K^-p amplitude. The full, dotted, dashed and dot-dashed lines visualize our results obtained with the parameter sets corresponding to $\sigma_{\pi N}$ terms set to 20, 30, 40 and 50 MeV, respectively.

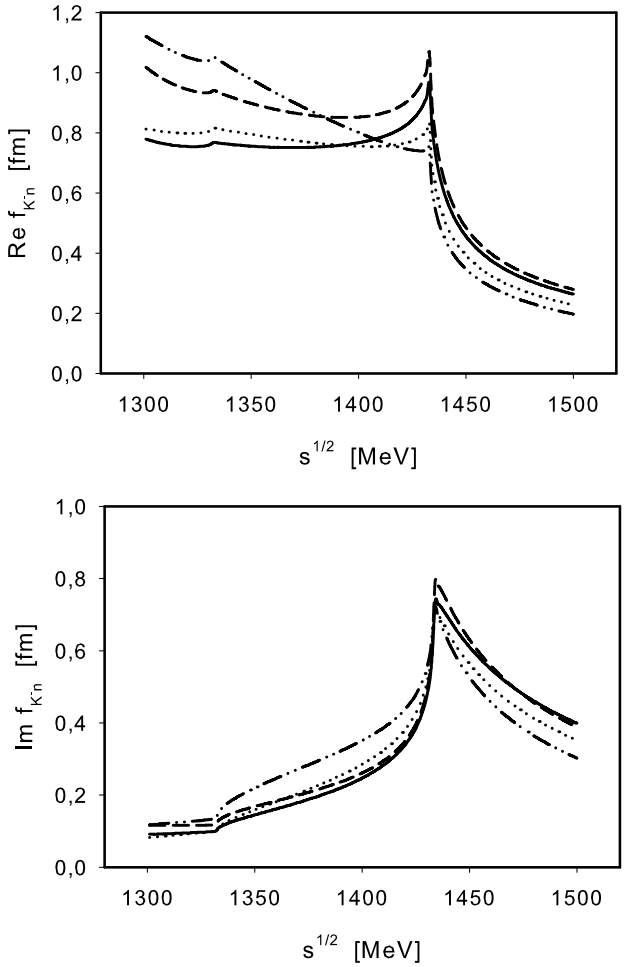

Fig. 5. The real (top panel) and imaginary (bottom panel) parts of the K^-n amplitude. The full, dotted, dashed and dot-dashed lines visualize our results obtained with the parameter sets corresponding to $\sigma_{\pi N}$ terms set to 20, 30, 40 and 50 MeV, respectively.

In Ref. [10] we also demonstrated that the K^-n amplitude obtained from multiple channel calculations with physical particle masses differs from the one derived by means of isospin relations from the transition amplitudes obtained in the K^-p sector. The reason is clear. Despite the underlying chiral Lagrangian adheres to the SU(3) symmetry and incorporates fully the isospin symmetry the use of physical masses breaks the symmetry. As the thresholds of the K^-p, K^-n and $\bar{K}^0n$ channels are different one cannot simply relate the K^-n amplitude to the isovector part of the K^-p amplitude. It also means that it may not be easy and straightforward to relate the K^--deuteron scattering length to the K^-N ones observed in experiments.

4 Concluding remarks

We have used effective chirally motivated separable potentials in simultaneous fits of the low energy K^-p cross sections, the threshold branching ratios and the characteristics of kaonic hydrogen. The fits are quite satisfactory except for the 1s level decay width being much larger than the experimental value. We have computed the characteristics of kaonic hydrogen (the 1s level energy shift and width) directly and emphasize that this approach is vital in view of the expected precision of the coming experimental data.

Our results confirm observations by other authors that the coupled channel chiral model provides us with two poles in the complex energy plane that can be related to the $\Lambda(1405)$ resonance observed in the $\pi\Sigma$ mass spectrum. However, we are not so convinced that both poles affect the physical observables as their positions seem to be model dependent and especially the one at higher energies may easily drift too far from the real axis. It is also intriguing that we were not able to get the position of any of the poles so close to the real axis as other authors claim. The disparity can be attributed most likely to the inclusion of the q^2 terms in the chiral Lagrangian and partly also to a different formulation of our model, namely to the use of ef-

fective separable potentials instead of the on-shell scheme employed in the inverse T-matrix approach.

We have also demonstrated the uncertainties related to extrapolation of the K^-N amplitudes to energies below the $\bar{K}N$ threshold. The variations between various approaches as well as between calculations performed with different parameter sets within a framework of a specific model can amount to tens of percents. A similar level of indefinitude should be anticipated in any calculation that incorporates the $\bar{K}N$ dynamics at energies below the $\bar{K}N$ threshold. In particular, this applies to theoretical treatment of the $\bar{K}NN$ bound state and to the kaonic nuclei in general.

We close our contribution by expressing a hope that the forthcoming high-precision data from the DEAR/SIDDHARTA collaboration and from experiments dedicated to the $\Lambda(1405)$ resonance will shred more light on kaon-nucleon dynamics and stimulate further theoretical work.

Acknowledgement: The authors acknowledge the financial support from the Grant Agency of the Czech Republic, grant 202/09/1441.

References

1. N. Kaiser, P. B. Siegel, and W. Weise, Nucl. Phys. **A 594** (1995) 325
2. E. Oset and A. Ramos, Nucl. Phys. **A 635** (1998) 99
3. A. Cieplý, E. Friedman, A. Gal, and J. Mareš, Nucl. Phys. **A 696** (2001) 173
4. B. Borasoy, R. Nißler, and W. Weise, Eur. Phys. J. **A 25** (2005) 79
5. B. Borasoy, U.-G. Meißner, and R. Nißler, Phys. Rev. **C 74** (2006) 055201
6. J. A. Oller, Eur. Phys. J. **A 28** (2006) 63
7. J. A. Oller and U.-G. Meißner, Phys. Lett. **B 500** (2001) 263
8. N. V. Shevchenko, A. Gal, J. Mareš, and J. Révai, Phys. Rev. **C 76** (2007) 044004
9. A. Cieplý and J. Smejkal, Eur. Phys. J. **A 34** (2007) 237
10. A. Cieplý and J. Smejkal, to appear in Eur. Phys. J. **A**, `arXiv:0910.1822 [nucl-th]` (2009)
11. M. Iwasaki *et al.*, Phys. Rev. Lett. **78** (1997) 3067; T. M. Ito *et al.*, Phys. Rev. **C 58** (1998) 2366
12. G. Beer *et al*. [DEAR Collab.], Phys. Rev. Lett. **94** (2005) 212302
13. A. D. Martin, Nucl. Phys. **B 179** (1981) 33; and earlier references cited therein
14. S. Deser, M. L. Goldberger, K. Baumann, and W. Thirring, Phys. Rev. **96** (1954) 774; T. L. Trueman, Nucl. Phys. **26** (1961) 57
15. U.-G. Meißner, U. Raha, and A. Rusetsky, Eur. Phys. J. **C 35** (2004) 349
16. C. Curceanu (Petrascu) *et al.*, *Proceedings of the MENU 2007 Conference, Jülich, Germany, September 10–14, 2007* (eds. H. Machner and S. Krewald), `eConf C070910` (2007) 102
17. P. G. Ratcliffe, Phys. Rev. **D 59** (1999) 014038
18. D. W. Thomas *et al.*, Nucl. Phys. **B 56** (1973) 15
19. R. J. Hemingway, Nucl. Phys. **B 253** (1984) 742
20. I. Zychor *et al.*, Phys. Lett. **B 660** (2008) 167
21. S. Prakhov *et al.*, Phys. Rev. **C 70** (2004) 034605
22. V. K. Magas, E. Oset, and A. Ramos, Phys. Rev. Lett. **95** (2005) 052301
23. D. Jido, J. A. Oller, E. Oset, A. Ramos, and U.-G. Meißner, Nucl. Phys. **A 725** (2003) 181
24. T. Hyodo and W. Weise, Phys. Rev. **C 77** (2008) 035204
25. T. Hyodo, S. I. Nam, D. Jido, and A. Hosaka, Phys. Rev. **C 68** (2003) 018201
26. A. Cieplý and A. Gal, `arXiv:0809.0422 [nucl-th]` (2008)